JBC RESEARCH ARTICLE

Liquid–liquid phase separation of the prion protein is regulated by the octarepeat domain independently of histidines and copper

Received for publication, December 27, 2023, and in revised form, April 12, 2024 Published, Papers in Press, April 22, 2024,
https://doi.org/10.1016/j.jbc.2024.107310

Janine Kamps[1,2], **Verian Bader**[1,3], **Konstanze F. Winklhofer**[2,3], **and Jörg Tatzelt**[1,2,*]

From the [1]*Department Biochemistry of Neurodegenerative Diseases, Institute of Biochemistry and Pathobiochemistry, Ruhr University Bochum, Bochum, Germany;* [2]*Cluster of Excellence RESOLV, Bochum, Germany;* [3]*Department Molecular Cell Biology, Institute of Biochemistry and Pathobiochemistry, Ruhr University Bochum, Bochum, Germany*

Reviewed by members of the JBC Editorial Board. Edited by Karen Fleming

Liquid-liquid phase separation (LLPS) of the mammalian prion protein is mainly driven by its intrinsically disordered N-terminal domain (N-PrP). However, the specific intermolecular interactions that promote LLPS remain largely unknown. Here, we used extensive mutagenesis and comparative analyses of evolutionarily distant PrP species to gain insight into the relationship between protein sequence and phase behavior. LLPS of mouse PrP is dependent on two polybasic motifs in N-PrP that are conserved in all tetrapods. A unique feature of mammalian N-PrP is the octarepeat domain with four histidines that mediate binding to copper ions. We now show that the octarepeat is critical for promoting LLPS and preventing the formation of PrP aggregates. Amphibian N-PrP, which contains the polybasic motifs but lacks a repeat domain and histidines, does not undergo LLPS and forms nondynamic protein assemblies indicative of aggregates. Insertion of the mouse octarepeat domain restored LLPS of amphibian N-PrP, supporting its essential role in regulating the phase transition of PrP. This activity of the octarepeat domain was neither dependent on the four highly conserved histidines nor on copper binding. Instead, the regularly spaced tryptophan residues were critical for regulating LLPS, presumably *via* cation–π interactions with the polybasic motifs. Our study reveals a novel role for the tryptophan residues in the octarepeat in controlling phase transition of PrP and indicates that the ability of mammalian PrP to undergo LLPS has evolved with the octarepeat in the intrinsically disordered domain but independently of the histidines.

A conformational transition of the cellular prion protein (PrP^C) into a β-sheet-rich isoform, denoted scrapie prion protein, causes prion diseases in humans and some other mammals. PrP^C is composed of a large intrinsically disordered N-terminal and a structured C-terminal domain, containing three alpha-helical regions and a short, two-stranded beta-sheet (1–3). Considering the evolution of PrP^C, it is interesting to note that the three-dimensional structure of the globular structured C-terminal domain of human (amino acid (aa) 121–230), chicken (aa 121–225), turtle (aa 121–225), and *Xenopus laevis* (aa 90–222) PrP^C shows extensive similarities, suggesting a conserved activity (4). In contrast, the N-terminal unstructured domain (N-PrP) is highly variable among tetrapod classes. This is in line with the observation that intrinsically disordered domains often evolve more rapidly than well-structured protein domains (5). Specifically, mammalian N-PrP contains glycine-rich octarepeats with conserved tryptophan, proline, and histidine residues in this region (6), while amphibian-PrP is devoid of any repeats and histidine residues (7) (Fig. 1, *A* and *B*). The mammalian octarepeat region is of particular interest in prion biology. Most importantly, extra octarepeat insertions in the PrP gene are associated with inherited prion diseases in humans (8–12) and a neurological illness in transgenic mice (13). On the molecular level, the four histidines of the octarepeat domain mediate an interaction of PrP with divalent metal ions such as copper, zinc, nickel, and manganese ions (14–18). The effects of copper binding and the histidines on conformation and function of PrP^C, as well as on the formation of scrapie prion protein, have been studied in more detail (19–27).

Several proteins linked to neurodegenerative diseases have the ability to form biomolecular condensates *via* LLPS, leading to a concept that condensates are precursors of neurotoxic protein aggregates (28–36). The mammalian PrP and N-terminal fragments thereof have been reported to undergo LLPS, pointing to a critical role of the N-terminal unstructured domain in regulating the phase separation of PrP (37–43). Indeed, in many cases, the activity to undergo LLPS is associated with the presence of intrinsically disordered domains with low complexity sequences that do not form stable folded structures (44, 45). Formation of biomolecular condensates of these domains is often driven by electrostatic (46, 47), π–π, cation–π (48–52), and hydrophobic (53) interactions. We have previously shown that two polybasic motifs located in the N- and C-terminal regions of N-PrP are required for LLPS, and since N-PrP contains no negatively charged residues, this effect is presumably due to cation–π interactions (42). Interestingly, the two polybasic motifs are highly conserved in all

* For correspondence: Jörg Tatzelt, Joerg.Tatzelt@rub.de.

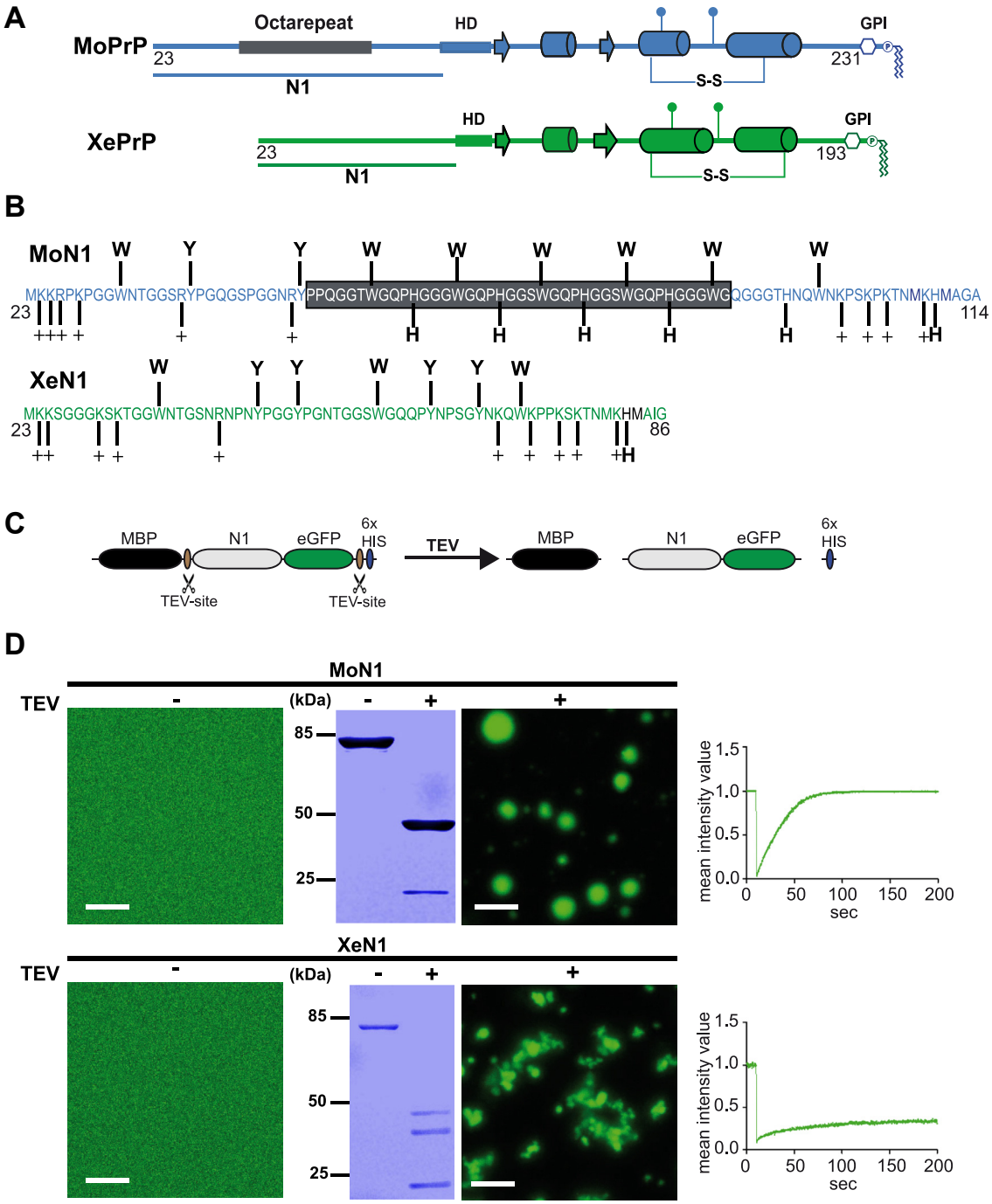

Figure 1. MoN1 undergoes LLPS, while XeN1 forms undynamic assemblies. *A*, schematic presentation of MoPrP (*blue*) and XePrP (*green*). Mouse octarepeat: *gray box*; *arrows*: beta strands; *tubes*: alpha helices. *B*, amino acid sequence of MoN1 and XeN1. Aromatic amino acids, positively charged amino acids, and histidines are highlighted. The presence of the histidine in XeN1 is due to the 3F4 epitope that was inserted to allow antibody detection of XePrP. Neither MoN1 nor XeN1 contains amino acids with negatively charged side chains. *C*, schematic presentation of the experimental approach. After expression in *Escherichia coli* and purification, phase separation is induced by removing the N-terminal maltose-binding protein (MBP) and C-terminal His tag (6x HIS) by incubation with TEV protease. *D*, MoN1-GFP and XeN1-GFP (10 μM in 10 mM Tris, pH 7.4) were analyzed by laser scanning microscopy before (TEV-) and after addition of TEV protease (TEV+). TEV protease cleavage was performed for 1 h. The scale bar represents 10 μm (*left panels*). An aliquot of each sample (4.5 μg) was analyzed in parallel by SDS-PAGE and Coomassie brilliant blue staining (*middle panels*). Protein mobility within the droplets was measured by fluorescence recovery after photobleaching (FRAP). After 10 s of baseline recording (pre-bleach), a small area of interest (AOI) was photobleached. The average normalized fluorescence intensity of three AOIs was plotted over time (*right panels*). C-C: disulphide bond; GPI: glycosylphosphatidylinositol anchor; HD, hydrophobic domain; LLPS, liquid-liquid phase separation; TEV, tobacco etch virus.

tetrapods including amphibian PrP (7, 54). To specifically investigate the role of the mammalian octarepeat in regulating phase transitions, we performed a comparative analysis of the unstructured N-terminal domains of mammalian PrP (MoN1) with that of amphibian PrP (XeN1), which lacks a repeat domain. Our study revealed that the mammalian octarepeat is

essential to promote the formation of biomolecular condensates *via* LLPS and to prevent protein aggregation. Strikingly, however, this activity did not depend on the histidines or on copper binding but rather on the regularly spaced tryptophan residues.

Results and discussion

Mouse N1-PrP but not Xenopus *N1-PrP undergoes LLPS*

To specifically address the role of the mammalian octarepeat in regulating phase transition of the intrinsically disordered N-terminal domain of PrP, we compared LLPS of *Mus musculus* N1 (MoN1) with that of *Xenopus laevis* N1 (XeN1), a naturally occurring N1-PrP lacking a repeat region (Fig. 1, *A* and *B*). Importantly, XeN1 harbors the two polybasic motifs that are important for LLPS of mouse PrP (42, 54). To study phase separation, we employed an *in vitro* system with purified proteins (42, 55, 56). This assay is based on PrP fusion proteins containing an N-terminal maltose-binding protein (MBP) to keep the recombinant proteins soluble and a C-terminal GFP to facilitate the microscopic analysis. After purification, the N-terminal MBP as well as the C-terminal His tag can be cleaved off by tobacco etch virus (TEV) protease to initiate phase transition (Fig. 1*C*). TEV-mediated release of MoN1 from MBP induced the rapid formation of highly dynamic assemblies, indicative of biomolecular condensates (Fig. 1*D* upper row) (42). XeN1 also underwent phase separation upon release of the MBP tag, but fluorescence recovery after photobleaching (FRAP) recordings revealed that the material properties of the XeN1 assemblies are different. In contrast to the liquid-like state of MoN1, the amphibian N1 was in a gel-like or aggregated state (Fig. 1*D*, lower row). These experiments suggested an essential role of the mammalian octarepeat in the ability of N1-PrP to form biomolecular condensates *via* LLPS. Interestingly, XeN1 did not remain soluble but forms irregular assemblies with a gel-like or aggregated state. Thus, the mammalian octarepeat seems to prevent a liquid-to-solid phase transition of N1-PrP by promoting LLPS and stabilizing liquid-like droplets.

LLPS of N1-PrP is controlled by the regularly spaced tryptophan residues in the octarepeat region and not by the histidines

To directly test that the octarepeat domain is causative for the differences in phase transition between mammalian and amphibian N1, we inserted the mouse octarepeat into *Xenopus* N1 (XeN1-MoOR). Indeed, the mouse octarepeat enabled amphibian N1 to form dynamic biomolecular condensates *via* LLPS. Based on FRAP recordings, it can be concluded that the XeN1-MoOR assemblies are liquid-like droplets, similarly to the the MoN1 assemblies (Fig. 2, *A* and *B*). To gain further insight into the association of protein sequence and phase behavior, we deleted conserved residues within the mammalian octarepeat. First, we replaced the four histidines in the octarepeat of mouse N1 by glycine residues. MoN1-ORΔH formed highly dynamic liquid-like assemblies, revealing that the histidines are dispensable for LLPS of MoN1 (Fig. 2*C*) (42).

Another notable feature of the mammalian octarepeat are five regularly spaced tryptophans that may promote LLPS through cation–π or π–π interactions. To test this hypothesis, we mutated and replaced five tryptophans by glycines both in mouse N1 and in the mouse-*Xenopus* N1 chimera. In contrast to MoN1 or XeN1-MoOR, MoN1-ORΔW and XeN1-ORΔW formed non-dynamic aggregates of irregular structure like amphibian N1 (Fig. 2, *D* and *E*). These findings provided the first evidence that the tryptophan residues in the mammalian octarepeat region have an important function in regulating phase transitions of PrP, whereas the histidines obviously do not play a major role in this pathway. In this context, it is interesting to note that the first repeat region that appeared in N1 during evolution is a hexarepeat in reptile PrP that contains only two histidines but already ten regularly spaced tyrosines (57). Similar to tryptophan, tyrosine can promote LLPS *via* cation–π or π–π interactions.

LLPS of full-length PrP is critically dependent on the tryptophans in the octarepeat region, but independent of copper

Having shown that the tryptophans, but not the histidines, within the octarepeat regulate LLPS of the N-terminally unstructured domain, we sought to verify these findings for full-length PrP. To this end, we generated two mouse PrP variants in which either the histidines (MoPrP-ORΔH) or the tryptophans (MoPrP-ORΔW) in the octarepeat were replaced by glycines. Fluorescence microscopy and FRAP recordings of phase-separated MoPrP-ORΔH and MoPrP-ORΔW confirmed the result we obtained with the isolated N-terminal domain. Replacing the histidine residues with glycines did not interfere with the LLPS of full-length MoPrP (Fig. 3, *A versus B*). It rather appeared that the MoPrP-ORΔH assemblies recovered faster than those formed by WT PrP. One possible explanation could be that the four missing histidine residues result in fewer π–π and cation–π interactions compared to WT PrP. This would lead to weaker intermolecular interactions and enhanced dynamicity. In contrast, the behavior of phase-separated full-length MoPrP with deleted tryptophans in the octarepeat was altered: the FRAP recordings revealed that MoPrP-ORΔW formed less dynamic gel-like or aggregated assemblies (Fig. 3*C*).

The histidines in the octarepeat domain have been shown to interact with copper. This raised the question of a possible role of copper binding in LLPS of PrP. To address this aspect, we purified WT mouse full-length PrP and N-PrP under copper-free conditions and then analyzed their phase transition in the absence or presence of 2, 5, or 10 μM $CuCl_2$. Based on the microscopic analysis, the phase separation behavior of both full-length PrP and N1-PrP was not influenced by copper (Fig. 3, *D* and *E*). In addition, a quantitative analysis confirmed no differences in droplet volume and sphericity between the condensates formed with or without $CuCl_2$ (Fig. 4*A*). Thus, these results suggest that copper ions are not required for LLPS of PrP and do not seem to modulate this process under physiological conditions.

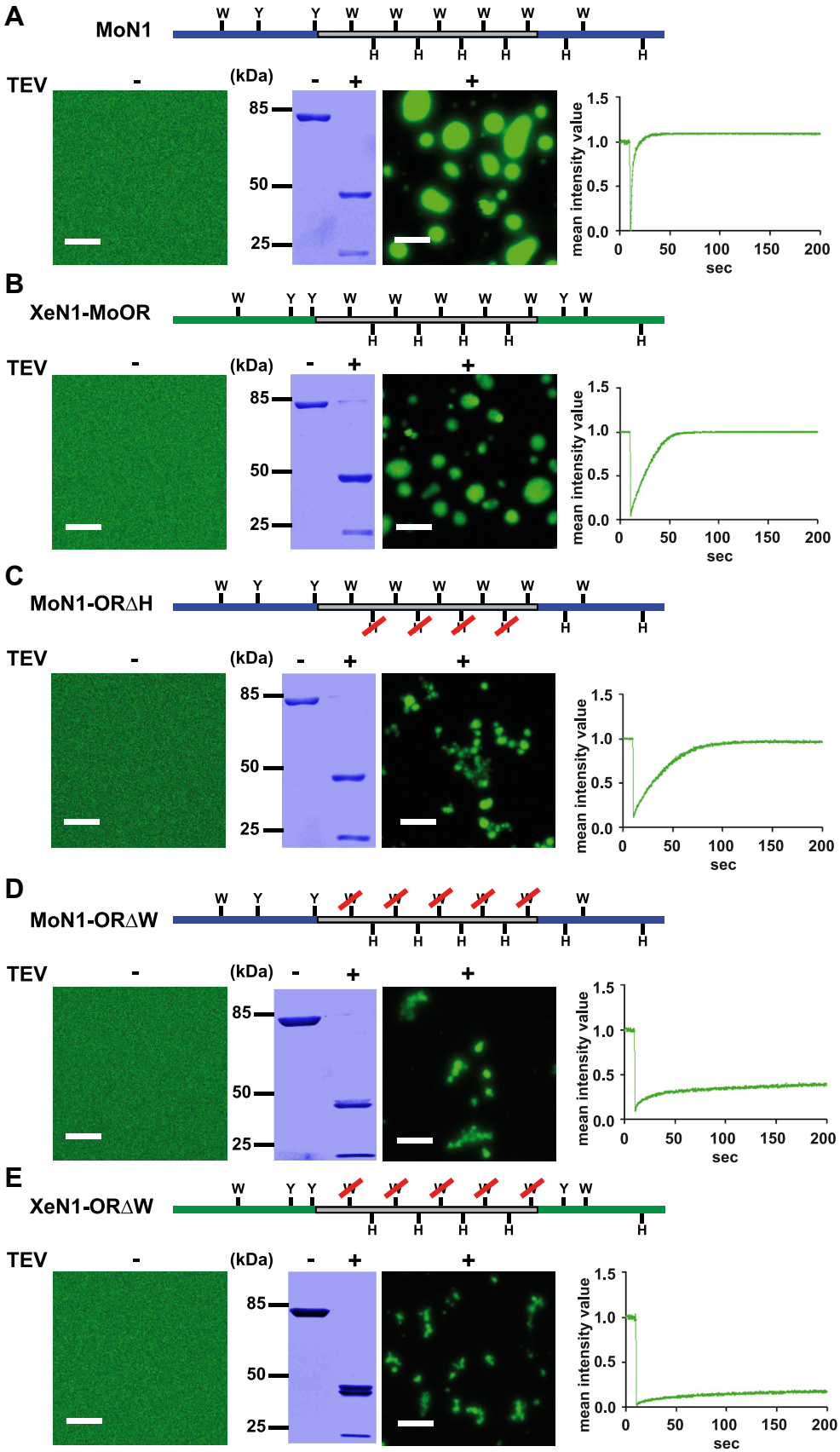

Figure 2. LLPS of N1PrP is controlled by the tryptophans within the octarepeat, but not by the histidines. *A*, schematic presentation of WT MoN1 (*top* panel). Ten μM of protein in 10 mM Tris, pH 7.4 was incubated for 1 h in the absence (TEV-) or presence (TEV+) of TEV protease and then analyzed by laser scanning microscopy. The scale bar represents 10 μm. An aliquot of each sample (4.5 μg) was analyzed in parallel by SDS-PAGE and Coomassie brilliant blue staining (*middle* panel). Protein mobility within the droplets was measured by fluorescence recovery after photobleaching (FRAP) as described in Figure 1*D*.

Taken together, in this study, we identified a sequence-encoded molecular grammar regulating liquid–liquid phase separation of the mammalian prion proteins. First, we found that the mammalian octarepeat domain is essential for LLPS of PrP. Surprisingly, the histidines, which are specific for mammalian PrP, are dispensable for LLPS, whereas the tryptophans are critical to promote LLPS and to prevent the formation of gel-like or aggregated structures. Considering that cation–π interactions of the aromatic residues in the octarepeat with the two polybasic motifs are the main driver of LLPS, it seems plausible that tryptophans can make stronger interactions than histidines. This may be the reason why the tryptophane deletions, but not the histidine deletions, interfere with LLPS. More broadly, our study also revealed that the octarepeat domain has a biological function independent of the histidines and copper binding. This raises the intriguing question of how the activity of tryptophans to regulate phase transition is involved in the physiological activity of PrP^C and the formation of pathological PrP conformers.

Experimental procedures

Plasmids and constructs

All plasmids were maintained and amplified in *Escherichia coli* TOP10 (Thermo Fisher scientific). The utilized constructs were created by standard cloning techniques. The mouse PrP constructs are based on the coding region of mouse PrP gene (Prnp; GenBank accession number M18070) and the frog PrP constructs are based on the coding region of *X. laevis* PrP gene (7) (GenBank accession number NM_001088711.1). Both sequences were changed to express PrP-L108M/V111M (58), to enable detection by mAb3F4 (59). N1 of mouse includes aa 23 to 114; N1 of *X. laevis* includes aa 23 to 86. XeN1-MoOR: insertion of mouse octarepeat domain (OR) (aa 50–89) between *X. laevis* Y49 and N62; MoN1-ORΔH: the four H in the mouse OR were changed to G; MoN1-ORΔW: the 5 W in the OR were changed to G; XeN1-ORΔW: insertion of mouse ORΔW between *X. laevis* Y49 and N62. The names, abbreviations, and sequences of all PrP constructs analyzed in this study are also summarized in Figure 4. The MBP-TEV-PrP-eGFP-TEV-His_6 plasmids were generated by switching the FUS coding region from pMal-TEV-FUS-eGFP-TEV-His_6 construct, kindly provided by Dorothee Dormann (60), to the respective PrP variants.

Protein expression and purification

Protein expression and purification was performed as previously described in (42). Shortly, MBP-N1-PrP-eGFP plasmids were transformed into BL21-DE3, and MBP-PrP-eGFP plasmids were transformed into Origami B (DE3) competent cells (Novagen). Then, 1 L of lysogeny broth medium was inoculated and grown to an absorbance (600 nm) of 0.9. Afterward, cultures were incubated for 30 min on ice. Expression was induced with 100 μM IPTG and incubated overnight at 12 °C, 120 rpm for BL21 cultures. Origami B culture expression was induced with 0.5 mM IPTG and incubated overnight at 25 °C, 120 rpm. Harvesting of bacteria was conducted at 5000*g*, 4 °C, 20 min. Subsequently, the pellet was washed with 20 ml Millipore water, centrifuged at 2000*g*, 4 °C, 20 min, and stored at −20 °C until further use. After this, the pellet was first resuspended in lysis buffer (50 mM Na_2HPO_4/NaH_2PO_4 (pH 8.0), 500 mM NaCl, 0.01 mM $ZnCl_2$, 10% glycerol) and lysed with SLM AMINCO French Press (Thermo Fisher Scientific). Following, the protein solution was centrifuged at 40,000*g*, 45 min, 4 °C. A His-Trap FF column (GE Healthcare) was equilibrated with lysis buffer, then protein was loaded and washed first with five CV lysis buffer containing 20 mM imidazole and second washed with three CV lysis buffer containing 50 mM imidazole. Elution was performed by lysis buffer containing 200 mM imidazole. After elution, the protein was dialyzed overnight in dialysis buffer (50 mM Na_2HPO_4/NaH_2PO_4 (pH 8.0), 500 mM NaCl, 0.01 mM $ZnCl_2$, 5% glycerol). Protein concentration was determined by NanoDrop 2000 (Thermo Fisher Scientific), aliquoted, and stored at − 80 °C. For the experiments studying the role of copper on LLPS, the purification buffers and dialysis buffer did not contain $ZnCl_2$. In addition, the dialysis buffer was supplemented with 1 mM EDTA to remove any possible attached metal ions.

Sample preparation

For sample preparation, the proteins were thawed on ice and centrifuged (20,000*g* for 10 min at 4 °C). To exchange the buffer to 10 mM Tris, pH 7.4, the solution was centrifuged (five times at 12,000*g* for 7 min at 4 °C) through Vivaspin 500 columns with 30-kDa molecular weight cut off (Sartorius Stedim biotech). Afterward, protein concentration was determined by NanoDrop 2000. Phase transition was initiated by adding TEV protease for 1 h to the samples. To analyze the effect of copper on PrP phase separation, we used a buffer with high-purity Tris-HCl from PanReac AppliChem. In addition, before every experiment, the protein solutions were tested for copper contamination with the Copper Assay Kit from Sigma-Aldrich. When no copper was detected with this kit, the corresponding protein solution was defined as copper free. To study the effect of increasing copper concentrations on LLPS, $CuCl_2$ was added to the reaction before TEV protease.

Laser scanning microscopy

Fluorescent imaging laser scanning microscopy was performed as described in (42). Imaging was conducted on an ELYRA PS.1 (Carl Zeiss) microscope with an imaging detector (LSM 880; Carl Zeiss). The 63x numerical aperture 1.4 oil-

B, schematic presentation of XeN1-MoOR, XeN1: *green*; *gray box*: mouse octarepeat. Fluorescence microscopy and FRAP recordings were performed as described in (*A*). *C*, schematic presentation of MoN1-ORΔH. Microscopic and FRAP analyses were performed as described in (*A*). *D*, schematic presentation of MoN1-ORΔW. Fluorescence microscopy and FRAP recordings were performed as described in (*A*). *E*, schematic presentation of XeN1-ORΔW. XeN1: *green*; *gray box*: mouse octarepeat. Fluorescence microscopy and FRAP recordings were performed as described in (*A*). LLPS, liquid-liquid phase separation; TEV, tobacco etch virus.

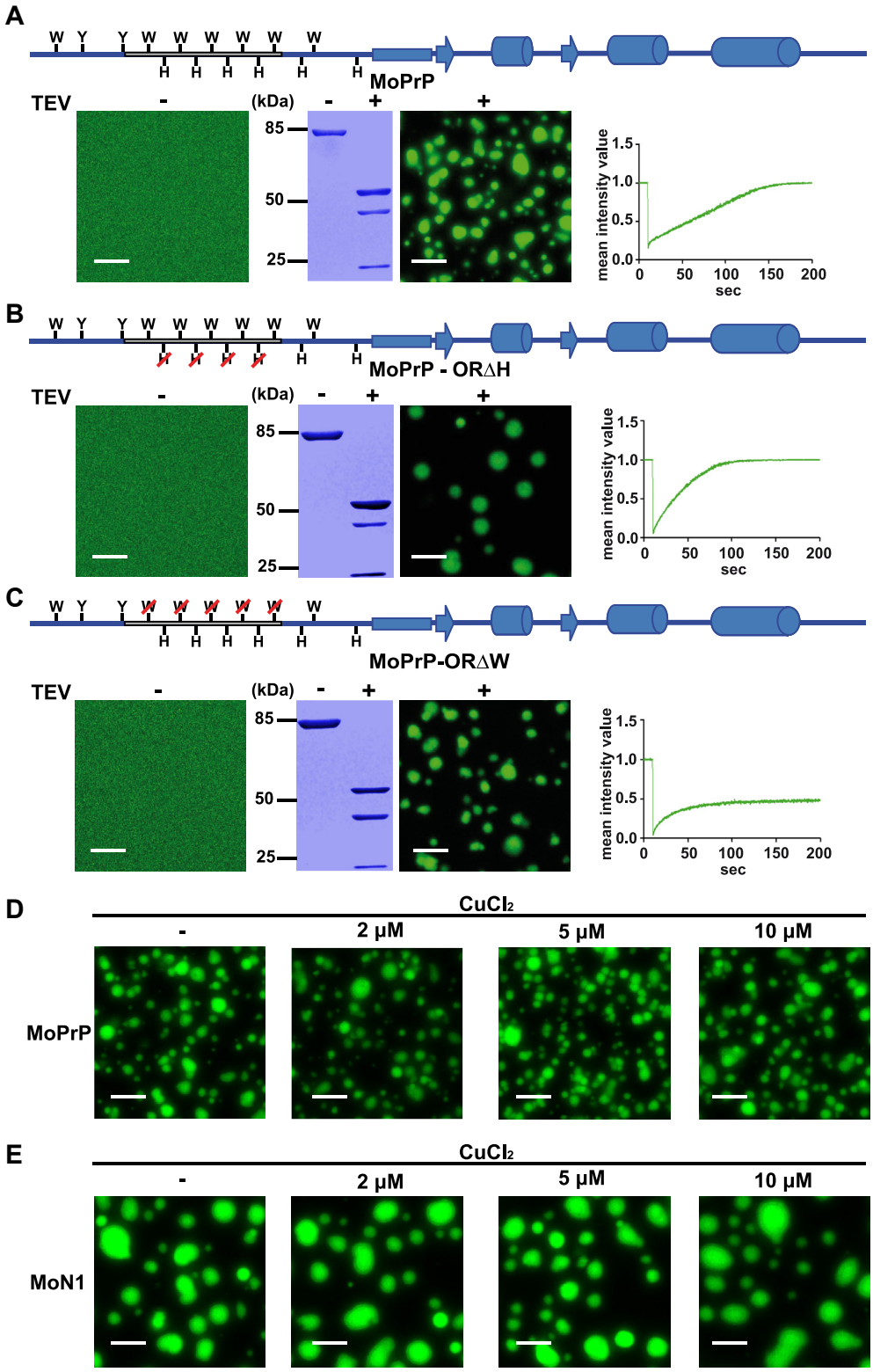

Figure 3. Liquid-liquid phase separation of full-length PrP is promoted by the tryptophans in the octarepeat and not influenced by copper. *A*, schematic presentation of WT MoPrP (*top panel*). Ten μM of MoPrP in 10 mM Tris, pH 7.4 was analyzed by laser scanning microscopy before (TEV-) or after (TEV+) incubation with TEV protease for 1 h. The scale bar represents 10 μm. An aliquot of each sample (4.5 μg) was analyzed in parallel by SDS-PAGE and Coomassie brilliant blue staining (*middle panels*). Protein mobility within the droplets was measured by fluorescence recovery after photobleaching (FRAP) as described in Figure 1*D*. *B*, schematic presentation of MoPrP-ORΔH. The histidine residues in the octarepeat were replaced by glycines. Fluorescence microscopy and FRAP recordings were performed as described in (*A*). *C*, schematic presentation of MoPrP-ORΔW. The tryptophanes in the octarepeat were replaced by glycines. Fluorescence microscopy and FRAP recordings were performed as described in (*A*). *D*, ten μM of WT MoPrP in 10 mM Tris–HCl, pH 7.4 containing increasing amounts of $CuCl_2$ as indicated was incubated with TEV protease for 1 h and then analyzed by laser scanning microscopy. The scale bar represents 10 μm. *E*, ten μM of WT MoN1 in 10 mM Tris–HCl, pH 7.4 containing increasing concentrations of $CuCl_2$ as indicated was incubated with TEV protease for 1 h and then analyzed by laser scanning microscopy. The scale bar represents 10 μm. TEV, tobacco etch virus.

A

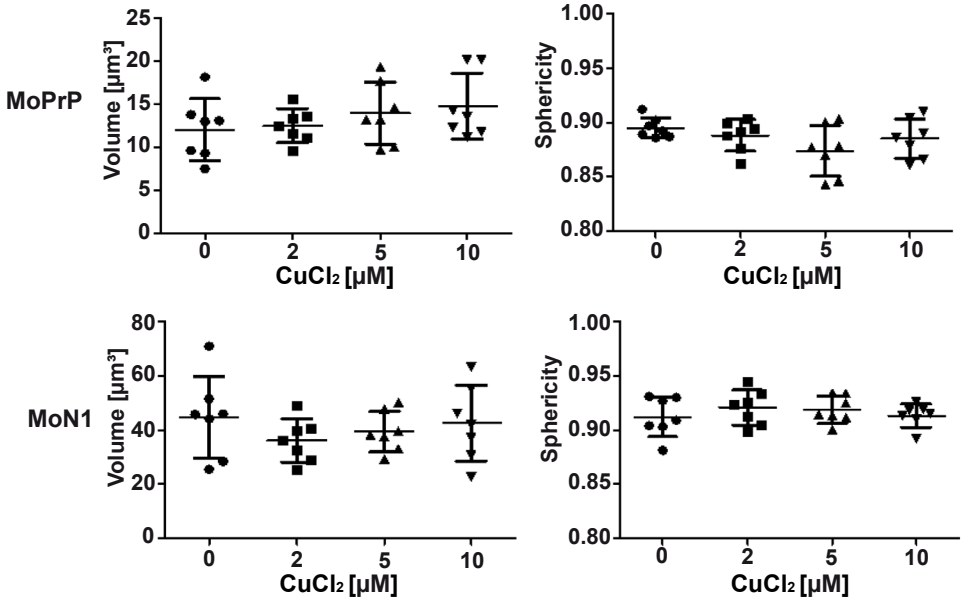

B

Protein	Abbreviation	Sequence
Mouse prion protein N-terminal domain	MoN1	MKKRPKPGGWNTGGSRYPGQGSPGGNRYPPQGGT**W**GQP**H**G GG**W**GQP**H**GGS**W**GQP**H**GGS**W**GQP**H**GGG**W**GQGGGTHNQWN KPSKPKTNMKHMAGA
X. laevis prion protein N-terminal domain	XeN1	MKKSGGGKSKTGGWNTGSNRNPNYPGGYPGNTGGSWGQQP YNPSGYNKQW KPPKSKTNMKHMAIG
X. laevis prion protein N-terminal domain with insertion of the mouse octarepeat (OR)	XeN1-MoOR	MKKSGGGKSKTGGWNTGSNRNPNYPGGYPPQGGT**W**GQP**H**G GG**W**GQP**H**GGS**W**GQP**H**GGS**W**GQP**H**GGG**W**GNPSGYNKQWK PPKSKTNMKHMAIG
Mouse prion protein N-terminal domain with Histidine residues in the OR exchanged to glycine residues	MoN1-ORΔH	MKKRPKPGGWNTGGSRYPGQGSPGGNRYPPQGGT**W**GQP**G**G GG**W**GQP**G**GGS**W**GQP**G**GGS**W**GQP**G**GGG**W**GQGGGTHNQW NKPSKPKTNMKHMAGA
Mouse prion protein N-terminal domain with Tryptophane residues in the OR exchanged to glycine residues	MoN1-ORΔW	MKKRPKPGGWNTGGSRYPGQGSPGGNRYPPQGGT**G**GQP**H**G GG**G**GQP**H**GGS**G**GQP**H**GGS**G**GQP**H**GGGG**G**QGGGTHNQWNK PSKPKTNMKHMAGA
X. laevis prion protein N-terminal domain with insertion of the mouse OR and Tryptophane residues in the OR exchanged to glycine residues	XeN1-ORΔW	MKKSGGGKSKTGGWNTGSNRNPNYPGGYPPQGGT**G**GQP**H**G GG**G**GQP**H**GGS**G**GQP**H**GGS**G**GQP**H**GGGG**G**NPSGYNKQWKP PKSKTNMKHMAIG
Mouse full length prion protein	MoPrP	MKKRPKPGGWNTGGSRYPGQGSPGGNRYPPQGGT**W**GQP**H**G GG**W**GQP**H**GGS**W**GQP**H**GGS**W**GQP**H**GGG**W**GQGGGTHNQWN KPSKPKTNMKHMAGAAAAGAVV GGLGGYMLGSAMSRPMIHFGNDWEDRYYRENMYRYPNQVYY RPVDQYSNQNNFVHDCVNITIKQHTVTTTTKGENFTETDVKMM ERVVEQMCVTQYQKESQAYYDGRRSS
Mouse full length prion protein with Histidine residues in the OR exchanged to glycine residues	MoPrP-ORΔH	MKKRPKPGGWNTGGSRYPGQGSPGGNRYPPQGGT**W**GQP**G**G GG**W**GQP**G**GGS**W**GQP**G**GGS**W**GQP**G**GGG**W**GQGGGTHNQW NKPSKPKTNMKHMAGAAAAGAVVGGLGGYMLGSAMSRPMIHF GNDWEDRYYRENMYRYPNQVYYRPVDQYSNQNNFVHDCVNIT IKQHTVTTTTKGENFTETDVKMMERVVEQMCVTQYQKESQAYY DGRRSS
Mouse full length prion protein with Tryptophane residues in the OR exchanged to glycine residues	MoPrP-ORΔW	MKKRPKPGGWNTGGSRYPGQGSPGGNRYPPQGGT**G**GQP**H**G GG**G**GQP**H**GGS**G**GQP**H**GGS**G**GQP**H**GGG**G**GQGGGTHNQWNK PSKPKTNMKHMAGAAAAGAVVGGLGGYMLGSAMSRPMIHFGN DWEDRYYRENMYRYPNQVYYRPVDQYSNQNNFVHDCVNITIK QHTVTTTTKGENFTETDVKMMERVVEQMCVTQYQKESQAYYD GRRSS

Figure 4. Copper does not influence volume and sphericity of PrP condensates. *A*, image quantifications of the condensates formed by MoPrP and MoN1 shown in Figure 3, *D* and *E*. Droplet surfaces were reconstructed using Imaris 10.1.0 surface module; droplet volume and sphericity were plotted against different $CuCl_2$ concentrations. Statistical analysis: Kolmogorov-Smirnov test followed by ANOVA with Dunnett's Multiple Comparison Test (n = 7 per condition from four independent experiments). *B*, the table summarizes the names, abbreviations, and amino acid sequences of the constructs used in this study. Mouse sequences are highlighted in *blue* and *Xenopus laevis* sequences in *green*. The octarepeat is marked in *gray* and the analyzed tryptophanes and histidines are shown in *bold* letters. Mutations are depicted in *red*.

immersion objective was utilized to record a z-stack of 67.5 × 67.5 × 10 µm and 0.900 µm for each optical section. The power of the argon laser was set to 0.006% at 488 nm with pixel dwell time of 5.71 µs. All settings were kept constant during the measurements. FRAP experiments were performed with the Plan-Apochromat 100x numerical aperture 1.46 oil differential interference contrast M27 objective and ZEN2.1 bleaching and region software module. Three circular regions with a 12-pixel diameter were utilized as regions of interest. Two regions were deployed as background signal and reference signal. The other region was bleached with 100% laser power and a pixel dwell time of 8.71 ms, with scan time of 111.29 ms and pixel dwell time of 1.61 ms. Excel 2016 was utilized for data evaluation and diagrams were designed in GraphPad Prism.

Data availability

All data are contained within the manuscript.

Acknowledgments—We are grateful to Petra Goldmann and Andrea Roth-Sturm for technical support. Confocal laser scanning and SR-SIM microscopy was funded by the German Research Foundation and the State Government of North Rhine-Westphalia (INST 213/840-1 FUGG).

Author contributions—J. K. and V. B. investigation; K. F. W. and J. T. conceptualization; J. K. and V. B. data curation; J. K. and V. B. methodology; J. K. and J. T. formal analysis; K. F. W. and J. T. writing–original draft; J. K., V. B., K. F. W., and J. T. writing–review and editing; J. K. and V. B. visualization; J. T. supervision; J. T. funding acquisition.

Funding and additional information—This work was funded by the Deutsche Forschungsgemeinschaft (DFG, German Research Foundation) under Germany's Excellence Strategy – EXC 2033 – 390677874 – RESOLV; TA 167/6-3 and TA 167/11-1 (to J. T.); WI/2111-6 (to K. F. W.).

Conflict of interest—The authors declare that they have no conflicts of interest with the contents of this article.

Abbreviations—The abbreviations used are: FRAP, fluorescence recovery after photobleaching; LLPS, liquid-liquid phase separation; MBP, maltose-binding protein; PrP^{C}, cellular prion protein; TEV, tobacco etch virus.

References

1. Donne, D. G., Viles, J. H., Groth, D., Mehlhorn, I., James, T. L., Cohen, F. E., *et al.* (1997) Structure of the recombinant full-length hamster prion protein PrP(29-231): the N terminus is highly flexible. *Proc. Natl. Acad. Sci. U. S. A.* **94**, 13452–13457
2. Riek, R., Hornemann, S., Wider, G., Billeter, M., Glockshuber, R., and Wuthrich, K. (1996) NMR structure of the mouse prion protein domain PrP(121-321). *Nature* **382**, 180–182
3. Riek, R., Hornemann, S., Wider, G., Glockshuber, R., and Wuthrich, K. (1997) NMR characterization of the full-length recombinant murine prion protein, mPrP(23-231). *FEBS Lett.* **413**, 282–288
4. Calzolai, L., Lysek, D. A., Perez, D. R., Guntert, P., and Wuthrich, K. (2005) Prion protein NMR structures of chickens, turtles, and frogs. *Proc. Natl. Acad. Sci. U. S. A.* **102**, 651–655
5. Brown, C. J., Takayama, S., Campen, A. M., Vise, P., Marshall, T. W., Oldfield, C. J., *et al.* (2002) Evolutionary rate heterogeneity in proteins with long disordered regions. *J. Mol. Evol.* **55**, 104–110
6. Oesch, B., Westaway, D., Wälchli, M., McKinley, M. P., Kent, S. B. H., Aebersold, R., *et al.* (1985) A cellular gene encodes scrapie PrP 27-30 protein. *Cell* **40**, 735–746
7. Strumbo, B., Ronchi, S., Bolis, L. C., and Simonic, T. (2001) Molecular cloning of the cDNA coding for Xenopus laevis prion protein. *FEBS Lett.* **508**, 170–174
8. Goldfarb, L. G., Brown, P., McCombie, W. R., Goldgaber, D., Swergold, G. D., Wills, P. R., *et al.* (1991) Transmissible familial Creutzfeldt-Jakob disease associated with five, seven, and eight extra octapeptide coding repeats in the PRNP gene. *Proc. Natl. Acad. Sci. U. S. A.* **88**, 10926–10930
9. Owen, F., Poulter, M., Collinge, J., Leach, M., Lofthouse, R., Crow, T. J., *et al.* (1992) A dementing illness associated with a novel insertion in the prion protein gene. *Brain Res. Mol. Brain Res.* **13**, 155–157
10. Owen, F., Poulter, M., Shah, T., Collinge, J., Lofthouse, R., Baker, H., *et al.* (1990) An in-frame insertion in the prion protein gene in familial Creutzfeldt-Jakob disease. *Brain Res. Mol. Brain Res.* **7**, 273–276
11. Hill, A. F., Joiner, S., Beck, J. A., Campbell, T. A., Dickinson, A., Poulter, M., *et al.* (2006) Distinct glycoform ratios of protease resistant prion protein associated with PRNP point mutations. *Brain* **129**, 676–685
12. Krasemann, S., Zerr, I., Weber, T., Poser, S., Kretzschmar, H., Hunsmann, G., *et al.* (1995) Prion disease associated with a novel nine octapeptide repeat insertion in the PRNP gene. *Brain Res. Mol. Brain Res.* **34**, 173–176
13. Chiesa, R., Piccardo, P., Ghetti, B., and Harris, D. A. (1998) Neurological illness in transgenic mice expressing a prion protein with an insertional mutation. *Neuron* **21**, 1339–1351
14. Jackson, G. S., Murray, I., Hosszu, L. L. P., Gibbs, N., Waltho, J. P., Clarke, A. R., *et al.* (2001) Location and properties of metal-binding sites on the human prion protein. *Proc. Natl. Acad. Sci. U. S. A.* **98**, 8531–8535
15. Treiber, C., Thompsett, A. R., Pipkorn, R., Brown, D. R., and Multhaup, G. (2007) Real-time kinetics of discontinuous and highly conformational metal-ion binding sites of prion protein. *J. Biol. Inorg. Chem.* **12**, 711–720
16. Pan, K., Yi, C. W., Chen, J., and Liang, Y. (2015) Zinc significantly changes the aggregation pathway and the conformation of aggregates of human prion protein. *Biochim. Biophys. Acta* **1854**, 907–918
17. Stöckel, J., Safar, J., Wallace, A. C., Cohen, F. E., and Prusiner, S. B. (1998) Prion protein selectively binds copper(II) ions. *Biochemistry* **37**, 7185–7193
18. Brown, D. R., Qin, K., Herms, J. W., Madlung, A., Manson, J., Strome, R., *et al.* (1997) The cellular prion protein binds copper in vivo. *Nature* **390**, 684–687
19. do Amaral, M. J., Mohapatra, S., Passos, A. R., Lopes da Silva, T. S., Carvalho, R. S., da Silva Almeida, M., *et al.* (2023) Copper drives prion protein phase separation and modulates aggregation. *Sci. Adv.* **9**, eadi7347
20. Bocharova, O. V., Breydo, L., Parfenov, A. S., Salnikov, V. V., and Baskakov, I. V. (2005) *In vitro* conversion of full-length mammalian prion protein produces amyloid form with physical properties of PrP(Sc). *J. Mol. Biol.* **346**, 645–659
21. Younan, N. D., Klewpatinond, M., Davies, P., Ruban, A. V., Brown, D. R., and Viles, J. H. (2011) Copper(II)-induced secondary structure changes and reduced folding stability of the prion protein. *J. Mol. Biol.* **410**, 369–382
22. Evans, E. G. B., and Millhauser, G. L. (2017) Copper- and zinc-promoted Interdomain structure in the prion protein: a mechanism for Autoinhibition of the neurotoxic N-terminus. *Prog. Mol. Biol. Transl. Sci.* **150**, 35–56
23. McDonald, A. J., Leon, D. R., Markham, K. A., Wu, B., Heckendorf, C. F., Schilling, K., *et al.* (2019) Altered domain structure of the prion protein caused by Cu(2+) binding and Functionally Relevant mutations: analysis by Cross-Linking, MS/MS, NMR. *Structure* **27**, 907–922.e905
24. Treiber, C., Pipkorn, R., Weise, C., Holland, G., and Multhaup, G. (2007) Copper is required for prion protein-associated superoxide dismutase-I activity in Pichia pastoris. *FEBS J.* **274**, 1304–1311

25. Sigurdsson, E. M., Brown, D. R., Alim, M. A., Scholtzova, H., Carp, R., Meeker, H. C., *et al.* (2003) Copper chelation delays the onset of prion disease. *J. Biol. Chem.* **278**, 46199–46202
26. Lau, A., McDonald, A., Daude, N., Mays, C. E., Walter, E. D., Aglietti, R., *et al.* (2015) Octarepeat region flexibility impacts prion function, endoproteolysis and disease manifestation. *EMBO Mol. Med.* **7**, 339–356
27. Eigenbrod, S., Frick, P., Bertsch, U., Mitteregger-Kretzschmar, G., Mielke, J., Maringer, M., *et al.* (2017) Substitutions of PrP N-terminal histidine residues modulate scrapie disease pathogenesis and incubation time in transgenic mice. *PLoS One* **12**, e0188989
28. Peskett, T. R., Rau, F., O'Driscoll, J., Patani, R., Lowe, A. R., and Saibil, H. R. (2018) A liquid to solid phase transition underlying pathological Huntingtin Exon1 aggregation. *Mol. Cell* **70**, 588–601.e586
29. Patel, A., Lee, H. O., Jawerth, L., Maharana, S., Jahnel, M., Hein, M. Y., *et al.* (2015) A liquid-to-solid phase transition of the ALS protein FUS Accelerated by disease mutation. *Cell* **162**, 1066–1077
30. Hardenberg, M. C., Sinnige, T., Casford, S., Dada, S. T., Poudel, C., Robinson, E. A., *et al.* (2021) Observation of an alpha-synuclein liquid droplet state and its maturation into Lewy body-like assemblies. *J. Mol. Cell Biol.* **13**, 282–294
31. Wegmann, S., Eftekharzadeh, B., Tepper, K., Zoltowska, K. M., Bennett, R. E., Dujardin, S., *et al.* (2018) Tau protein liquid-liquid phase separation can initiate tau aggregation. *EMBO J.* **37**, e98049
32. Molliex, A., Temirov, J., Lee, J., Coughlin, M., Kanagaraj, A. P., Kim, H. J., *et al.* (2015) Phase separation by low complexity domains promotes stress granule assembly and drives pathological fibrillization. *Cell* **163**, 123–133
33. Alberti, S., and Dormann, D. (2019) Liquid-liquid phase separation in disease. *Annu. Rev. Genet.* **53**, 171–194
34. Babinchak, W. M., and Surewicz, W. K. (2020) Liquid-liquid phase separation and its mechanistic role in pathological protein aggregation. *J. Mol. Biol.* **432**, 1910–1925
35. Darling, A. L., and Shorter, J. (2021) Combating deleterious phase transitions in neurodegenerative disease. *Biochim. Biophys. Acta Mol. Cell Res.* **1868**, 118984
36. Zbinden, A., Perez-Berlanga, M., De Rossi, P., and Polymenidou, M. (2020) Phase separation and neurodegenerative diseases: a disturbance in the force. *Dev. Cell* **55**, 45–68
37. Tange, H., Ishibashi, D., Nakagaki, T., Taguchi, Y., Kamatari, Y. O., Ozawa, H., *et al.* (2021) Liquid-liquid phase separation of full-length prion protein initiates conformational conversion in vitro. *J. Biol. Chem.* **296**, 100367
38. Huang, J. J., Li, X. N., Liu, W. L., Yuan, H. Y., Gao, Y., Wang, K., *et al.* (2020) Neutralizing mutations significantly Inhibit amyloid formation by human prion protein and decrease its cytotoxicity. *J. Mol. Biol.* **432**, 828–844
39. Matos, C. O., Passos, Y. M., do Amaral, M. J., Macedo, B., Tempone, M. H., Bezerra, O. C. L., *et al.* (2020) Liquid-liquid phase separation and fibrillation of the prion protein modulated by a high-affinity DNA aptamer. *FASEB J.* **34**, 365–385
40. Kostylev, M. A., Tuttle, M. D., Lee, S., Klein, L. E., Takahashi, H., Cox, T. O., *et al.* (2018) Liquid and Hydrogel phases of PrP(C) linked to conformation Shifts and Triggered by Alzheimer's amyloid-beta Oligomers. *Mol. Cell* **72**, 426–443.e412
41. Passos, Y. M., do Amaral, M. J., Ferreira, N. C., Macedo, B., Chaves, J. A. P., de Oliveira, V. E., *et al.* (2021) The interplay between a GC-rich oligonucleotide and copper ions on prion protein conformational and phase transitions. *Int. J. Biol. Macromol.* **173**, 34–43
42. Kamps, J., Lin, Y. H., Oliva, R., Bader, V., Winter, R., Winklhofer, K. F., *et al.* (2021) The N-terminal domain of the prion protein is required and sufficient for liquid-liquid phase separation: a crucial role of the Abeta-binding domain. *J. Biol. Chem.* **297**, 100860
43. Agarwal, A., Rai, S. K., Avni, A., and Mukhopadhyay, S. (2021) An intrinsically disordered pathological prion variant Y145Stop converts into self-seeding amyloids via liquid-liquid phase separation. *Proc. Natl. Acad. Sci. U. S. A.* **118**, e2100968118
44. Darling, A. L., Liu, Y., Oldfield, C. J., and Uversky, V. N. (2018) Intrinsically disordered Proteome of human Membrane-less organelles. *Proteomics* **18**, e1700193
45. Brangwynne, C. P., Tompa, P., and Pappu, R. V. (2015) Polymer physics of intracellular phase transitions. *Nat. Phys.* **11**, 899–904
46. Pak, C. W., Kosno, M., Holehouse, A. S., Padrick, S. B., Mittal, A., Ali, R., *et al.* (2016) Sequence Determinants of Intracellular phase separation by Complex coacervation of a disordered protein. *Mol. Cell* **63**, 72–85
47. Lin, Y. H., Forman-Kay, J. D., and Chan, H. S. (2016) Sequence-specific Polyampholyte phase separation in membraneless organelles. *Phys. Rev. Lett.* **117**, 178101
48. Kang, J., Lim, L., Lu, Y., and Song, J. (2019) A unified mechanism for LLPS of ALS/FTLD-causing FUS as well as its modulation by ATP and oligonucleic acids. *PLoS Biol.* **17**, e3000327
49. Das, S., Lin, Y. H., Vernon, R. M., Forman-Kay, J. D., and Chan, H. S. (2020) Comparative roles of charge, pi, and hydrophobic interactions in sequence-dependent phase separation of intrinsically disordered proteins. *Proc. Natl. Acad. Sci. U. S. A.* **117**, 28795–28805
50. Nott, T. J., Petsalaki, E., Farber, P., Jervis, D., Fussner, E., Plochowietz, A., *et al.* (2015) Phase transition of a disordered nuage protein generates environmentally responsive membraneless organelles. *Mol. Cell* **57**, 936–947
51. Kim, S., Huang, J., Lee, Y., Dutta, S., Yoo, H. Y., Jung, Y. M., *et al.* (2016) Complexation and coacervation of like-charged polyelectrolytes inspired by mussels. *Proc. Natl. Acad. Sci. U. S. A.* **113**, E847–E853
52. Sherrill, C. D. (2013) Energy component analysis of pi interactions. *Acc. Chem. Res.* **46**, 1020–1028
53. Yeo, G. C., Keeley, F. W., and Weiss, A. S. (2011) Coacervation of tropoelastin. *Adv. Colloid Interf. Sci.* **167**, 94–103
54. Polido, S. A., Kamps, J., and Tatzelt, J. (2021) Biological functions of the intrinsically disordered N-terminal domain of the prion protein: a possible role of liquid-liquid phase separation. *Biomolecules* **11**, 1201
55. Polido, S. A., Stuani, C., Voigt, A., Banik, P., Kamps, J., Bader, V., *et al.* (2023) Cross-seeding by prion protein inactivates TDP-43. *Brain* **147**, 240–254
56. Ramos, S., Kamps, J., Pezzotti, S., Winklhofer, K. F., Tatzelt, J., and Havenith, M. (2023) Hydration makes a difference! How to tune protein complexes between liquid-liquid and liquid-solid phase separation. *Phys. Chem. Chem. Phys.* **25**, 28063–28069
57. Simonic, T., Duga, S., Strumbo, B., Asselta, R., Ceciliani, F., and Ronchi, S. (2000) cDNA cloning of turtle prion protein. *FEBS Lett.* **469**, 33–38
58. Winklhofer, K. F., Heller, U., Reintjes, A., and Tatzelt, J. (2003) Inhibition of complex glycosylation increases formation of PrPSc. *Traffic* **4**, 313–322
59. Kascsak, R. J., Rubenstein, R., Merz, P. A., Tonna-DeMasi, M., Fersko, R., Carp, R. I., *et al.* (1987) Mouse polyclonal and monoclonal antibody to scrapie-associated fibril proteins. *J. Virol.* **61**, 3688–3693
60. Hofweber, M., Hutten, S., Bourgeois, B., Spreitzer, E., Niedner-Boblenz, A., Schifferer, M., *et al.* (2018) Phase separation of FUS is suppressed by its nuclear import receptor and arginine methylation. *Cell* **173**, 706–719.e713